JOURNAL OF GEOPHYSICAL RESEARCH, VOL. 114, G04003, doi:10.1029/2008JG000881, 2009

Interannual variability in atmospheric CO_2 uptake on the northeast U.S. continental shelf

Michael Previdi,[1] Katja Fennel,[2] John Wilkin,[3] and Dale Haidvogel[3]

Received 28 October 2008; revised 28 May 2009; accepted 13 July 2009; published 27 October 2009.

[1] Continental shelf systems are thought to play an important role in the exchange of carbon dioxide (CO_2) between the atmosphere and ocean. Currently, our ability to quantify the air-sea flux of CO_2 on continental shelves is limited due to large spatial and temporal variability coupled with historically sparse oceanographic measurements (e.g., of surface water pCO_2). Here we use the Regional Ocean Modeling System (ROMS) to quantify the air-sea flux of CO_2 and its interannual variability on the northeast U.S. continental shelf, which includes the Middle Atlantic Bight (MAB) and Gulf of Maine (GOM). Two years marked by opposite phases of the North Atlantic Oscillation (NAO) are considered in the study. A novel analysis method, second-order Taylor series decomposition, is used to identify the important processes responsible for producing NAO-related changes in the CO_2 air-sea flux. On the northeast U.S. shelf, atmospheric CO_2 uptake as simulated by ROMS decreases from 2.4 Mt C yr^{-1} in 1985 (low NAO) to 1.8 Mt C yr^{-1} in 1990 (high NAO), with most of this decrease (0.5 Mt C yr^{-1}) occurring in the MAB. In the MAB the difference in annual air-sea flux of CO_2 is due mainly to changes in near-surface wind speed, while the flux difference in the GOM is controlled primarily by surface water pCO_2 (CO_2 partial pressure) changes resulting from changes in sea surface temperature and new production. The large magnitude of interannual variability in the air-sea flux of CO_2 simulated here suggests the potential for even more significant flux changes in the future as climate change accelerates.

Citation: Previdi, M., K. Fennel, J. Wilkin, and D. Haidvogel (2009), Interannual variability in atmospheric CO_2 uptake on the northeast U.S. continental shelf, *J. Geophys. Res.*, *114*, G04003, doi:10.1029/2008JG000881.

1. Introduction

[2] The composition of Earth's atmosphere is one of the fundamental determinants of its climate. Greenhouse gases such as water vapor and carbon dioxide (CO_2) are effective absorbers and emitters of terrestrial (longwave) radiation, and help to maintain higher surface temperatures than would occur in the absence of these gases. CO_2, in particular, has received considerable attention in recent years, due in large part to the fact that its atmospheric concentration is strongly tied to human activity. Anthropogenic fossil fuel burning (and to a lesser extent other activities such as land use change) has resulted in a steady increase in atmospheric CO_2 concentration from about 280 parts per million (ppm) at the start of the industrial revolution to around 380 ppm today [*Forster et al.*, 2007]. This increase in atmospheric CO_2 has been concurrent with an increase in global mean surface temperature of about 0.7°C $century^{-1}$ during the past 100 years, with a rate of increase almost twice as large during the past 50 years [*Trenberth et al.*, 2007]. The future state of the climate will likewise depend critically on the amount of CO_2 present in the atmosphere, which will be influenced by human actions, but which will also depend on how the various other sources and sinks of CO_2 change as the climate changes.

[3] The global ocean is an important sink for anthropogenic CO_2. Estimates of oceanic CO_2 uptake vary, but are generally around 2 Pg C yr^{-1} [e.g., *Sarmiento and Gruber*, 2002; *Takahashi et al.*, 2002; *Bindoff et al.*, 2007]. It is not currently known how this uptake will respond to climatic change. The solubility of CO_2 in the surface water of the ocean decreases with increasing sea surface temperature (SST) and decreasing pH, implying that as the global ocean warms and becomes more acidic in a changing climate there will be less potential to draw down anthropogenic CO_2. Additionally, most coupled atmosphere-ocean models suggest that global warming will be accompanied by a weakening of the ocean's thermohaline circulation and associated reduction in the rate of mixing between surface and deep waters [*Meehl et al.*, 2007], which would tend to reduce oceanic CO_2 uptake by decreasing the effective volume of the ocean that is exposed to the atmosphere. Changes in SST, pH and vertical mixing could also affect the biological component of the ocean's carbon cycle [e.g., *Sarmiento et al.*, 2004], which might have further implications for the uptake of anthropogenic CO_2. Coupled climate-carbon cycle models

[1] Lamont-Doherty Earth Observatory, Columbia University, Palisades, New York, USA.
[2] Department of Oceanography, Dalhousie University, Halifax, Nova Scotia, Canada.
[3] Institute of Marine and Coastal Sciences, Rutgers University, New Brunswick, New Jersey, USA.

0148-0227/09/2008JG000881$09.00

indicate a reduced efficiency of the ocean to absorb anthropogenic CO_2 as the climate warms [*Friedlingstein et al.*, 2006]. This combined with reduced uptake capacity of the terrestrial biosphere results in a larger fraction of anthropogenic CO_2 remaining airborne, which acts to enhance global warming by the end of the 21st century by 0.1° to 1.5°C (relative to the case with no climate-carbon cycle feedback) [*Friedlingstein et al.*, 2006].

[4] Continental shelf systems play an important role in ocean carbon cycling even though they account for only about 7% of the surface area of the world ocean [*Gattuso et al.*, 1998]. Shelves receive large nutrient input from land and from the adjacent deep ocean and are the site for 14–30% of oceanic primary production [*Gattuso et al.*, 1998]. Several studies have also suggested that continental shelves may be an important sink for atmospheric CO_2 [e.g., *Tsunogai et al.*, 1999; *Frankignoulle and Borges*, 2001; *DeGrandpre et al.*, 2002; *Thomas et al.*, 2004]. *Tsunogai et al.* [1999] proposed a "continental shelf pump" paradigm to explain this CO_2 uptake. They postulated that enhanced cooling on the shallow shelf in winter relative to the open ocean would promote efficient absorption of atmospheric CO_2. (Biological production of organic matter on the shelf would further promote CO_2 uptake.) Exchange of shelf water with the deep ocean would then transport organic and inorganic carbon to the latter, maintaining relatively low surface water CO_2 concentrations on the shelf and thus allowing for continued drawdown of atmospheric CO_2. The physical transport of carbon to the deep ocean is critical to the continental shelf pump. Without this transport, surface water CO_2 concentrations on the shelf would increase in response to organic matter remineralization or seasonal warming or upwelling of carbon-rich waters [e.g., *Feely et al.*, 2008], resulting in little, if any, net uptake of CO_2 on the shelf in the course of a year.

[5] The notion that continental shelves are a sink for atmospheric CO_2 is highly debated. For example, *Cai et al.* [2003] and *Wang et al.* [2005] concluded that the U.S. South Atlantic Bight (SAB) behaves as a source of CO_2 to the atmosphere. This is in contrast to the more recent work of *Jiang et al.* [2008] that found the SAB to be a CO_2 sink. The debate over the source/sink status of continental shelves is critically important given the potentially large magnitude of CO_2 fluxes in shelf systems relative to the total CO_2 uptake by the world ocean. For instance, *Tsunogai et al.* [1999] estimated that the world continental shelf zone could absorb atmospheric CO_2 at the rate of 1 Pg C yr^{-1}, which is roughly half of the current uptake of anthropogenic CO_2 by the global ocean. Clearly, there is a need to be able to better quantify air-sea fluxes of CO_2 in ocean margins in order to better understand the role of the ocean in the global carbon cycle and thus climate change.

[6] The uncertainty regarding the role of continental shelves in the air-sea exchange of CO_2 stems largely from the fact that this exchange is so variable in both space and time. *Borges et al.* [2005] and *Cai et al.* [2006] begin to account for some of the spatial variability in the CO_2 flux by differentiating continental shelf systems based on their latitude. They suggest that low-latitude continental shelves are a source of CO_2 to the atmosphere, while those at mid to high latitudes are a CO_2 sink. A given shelf system, however, may behave differently as a CO_2 source or sink from one year to the next as a result of climate variability. For example, *Arrigo and Van Dijken* [2007] found that atmospheric CO_2 uptake by the Ross Sea, Antarctica varies by more than a factor of 20 between years as a result of changing sea ice cover. Quantifying interannual variability is therefore a critical component of the estimation of CO_2 fluxes on continental shelves.

[7] The current work quantifies interannual variations in the air-sea exchange of CO_2 for the northeast U.S. continental shelf, which includes the Middle Atlantic Bight (MAB) and Gulf of Maine (GOM). We use the Regional Ocean Modeling System (ROMS), a coupled physical-biogeochemical ocean model employed here for a domain that includes the northeast U.S. continental shelf and adjacent deep ocean (Figure 1a). ROMS is forced with atmospheric conditions characteristic of the high and low (i.e., positive and negative) phases of the North Atlantic Oscillation (NAO), which is the leading mode of climate variability in the northeast U.S. shelf region on interannual timescales [*Hurrell et al.*, 2003]. Differences in the annually integrated CO_2 air-sea flux between NAO extremes are discussed and attributed to accompanying changes in various physical and biological properties of the coupled air-sea system (e.g., SST, biological production of organic matter, near-surface wind speed). The exchange of CO_2 between the atmosphere and ocean has previously been investigated for the MAB by *DeGrandpre et al.* [2002], using observational data, and by *Fennel et al.* [2008] using ROMS. Both studies found the MAB to be a net annual sink for atmospheric CO_2 with a magnitude of about 1–2 Mt C yr^{-1}. *Fennel et al.* [2008] reached this conclusion after examining ROMS output for a single year (2004). *DeGrandpre et al.* [2002] compiled available surface water pCO_2 (CO_2 partial pressure) measurements from the years 1994–2000. The uncertainty associated with their estimate of the CO_2 flux therefore partially accounts for the effects of interannual variability; however, the uncertainty also arises due to other factors (e.g., the use of coarse spatial resolution pCO_2 measurements). Furthermore, it is questionable whether the seven year period of available observations fully spans the range of interannual variability. (For example, the NAO was observed to be mainly positive or neutral in this time frame.) The use of high spatial and temporal resolution model fields in the present study allows us to minimize uncertainty associated with sampling coverage when estimating the CO_2 air-sea flux. Additionally, by selecting years that were marked by opposite phases of the NAO, we can estimate the potential interannual variability of the flux in the region of interest resulting from interannual changes in the atmospheric forcing.

[8] The remainder of this paper is organized as follows. Section 2 describes the ROMS model and the design of the model experiments. In section 3, model output is compared with available observations. Section 4 discusses the simulated interannual difference in the CO_2 air-sea flux on the northeast U.S. continental shelf and the reasons for this difference. Finally, in section 5, the work is summarized and conclusions are presented.

2. Model Description and Experiment Design

2.1. ROMS Dynamics and Biogeochemical Submodels

[9] ROMS (http://www.myroms.org) is a free-surface, hydrostatic primitive equation ocean model [*Haidvogel et*

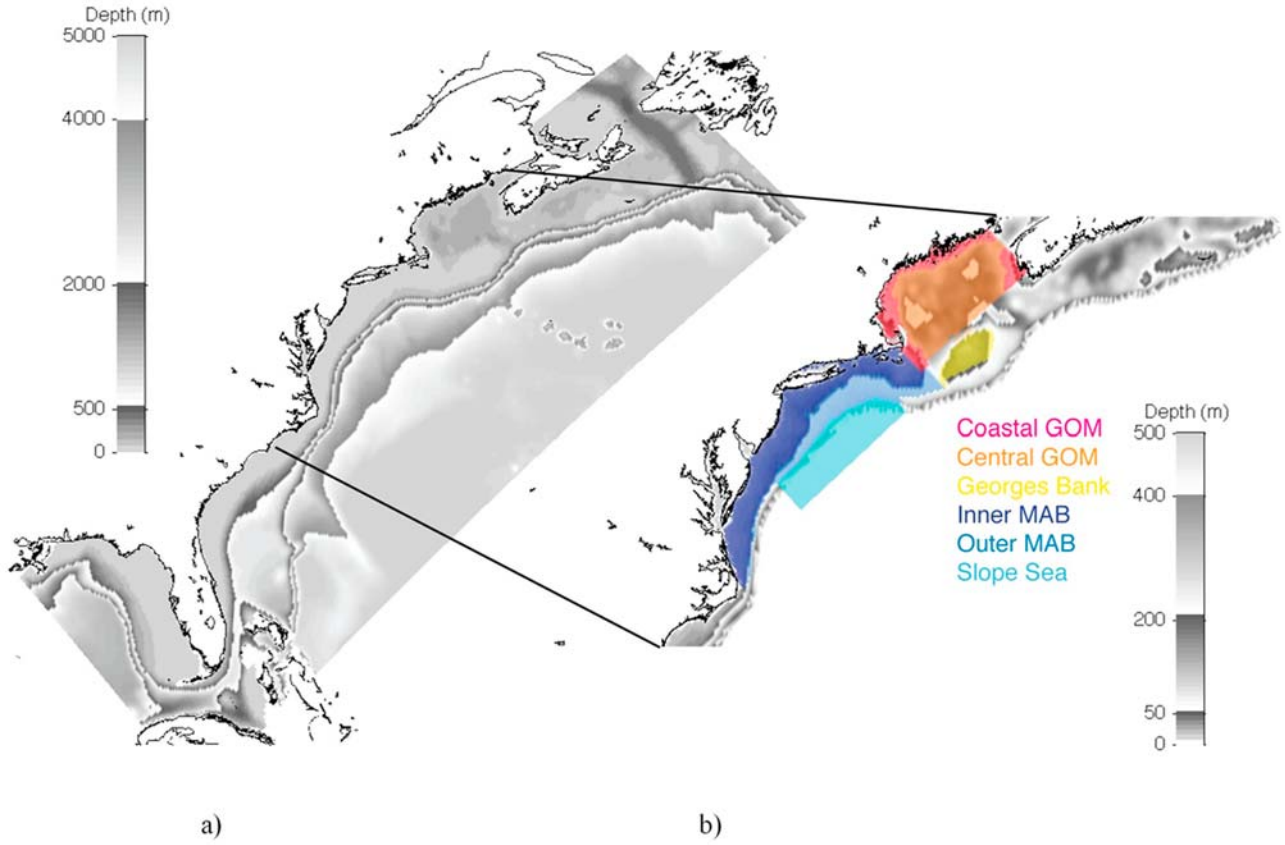

Figure 1. (a) ROMS NorthEast North American (NENA) domain. (b) Various subregions of the MAB/GOM and adjacent ocean, including the inner and outer MAB, MAB slope sea, coastal and central GOM, and Georges Bank.

al., 2008]. In the horizontal, the primitive equations are solved in orthogonal curvilinear coordinates on a staggered Arakawa C grid. The equations are discretized in the vertical using stretched terrain-following "s coordinates" that allow for increased resolution in areas of interest, such as near the thermocline, in bottom boundary layers, or, as in the present application, in the model euphotic zone. ROMS has several options for horizontal and vertical subgrid-scale mixing parameterizations. In the current model configuration, the horizontal mixing of momentum is on s coordinate surfaces, while horizontal mixing of tracers (e.g., temperature, salinity) is along geopotential (i.e., constant depth) surfaces. Vertical mixing of momentum and tracers is based on the 2.5-order turbulence closure method of *Mellor and Yamada* [1982]. Air-sea fluxes of momentum and latent and sensible heat in ROMS are parameterized using the bulk formulae of *Fairall et al.* [2003].

[10] ROMS includes a nitrogen-based biological model similar to the widely applied Fasham model [*Fasham et al.*, 1990]. The biological model includes seven state variables: phytoplankton (*Phy*), zooplankton (*Zoo*), nitrate (NO_3), ammonium (NH_4), small and large detritus (*SDet* and *LDet*, respectively), and phytoplankton chlorophyll (*Chl*). *Fennel et al.* [2006] present the equations governing the time rates of change of these variables, and describe in detail the modifications made to the Fasham model before its implementation in ROMS. The effects of benthic nitrogen cycling are accounted for by including explicit sediment denitrification in the biological model. Denitrification in sediments results in a flux of inorganic nutrients into the overlying water column which compensates for the flux of sinking organic matter out of the bottommost model grid box, thus coupling the pelagic and benthic aspects of the nitrogen cycle [*Fennel et al.*, 2006].

[11] Carbon is linked to the nitrogen cycle through photosynthesis (sink of inorganic carbon) and through different heterotrophic processes such as zooplankton excretion and microbial degradation of organic matter (sources of inorganic carbon). Accounting for these various biological sources and sinks along with the physical transport (advection and diffusion) of inorganic carbon within the water column and the air-sea gas exchange allows us to write the local rate of change of dissolved inorganic carbon (DIC) in the top model grid box of thickness Δz as

$$\begin{aligned}\frac{\partial DIC}{\partial t} = & -CN_{Phy}\cdot\mu\cdot Phy + \left(l_{BM} + l_E\frac{Phy^2}{k_p + Phy^2}\beta\right)\cdot CN_{Zoo} \\ & \cdot Zoo + CN_{Det}\cdot r_{SD}\cdot SDet + CN_{Det}\cdot r_{LD}\cdot LDet \\ & + \frac{kw^2}{Sc^{1/2}\Delta z}CO_{2,sol}\left(pCO_{2,air} - pCO_{2,sea}\right) \\ & + \nabla DIC\cdot\underline{V} + D_{DIC} \end{aligned} \quad (1)$$

where CN_{Phy}, CN_{Zoo}, and CN_{Det} are the carbon to nitrogen ratios of *Phy*, *Zoo*, and both *SDet* and *LDet*, respectively, μ

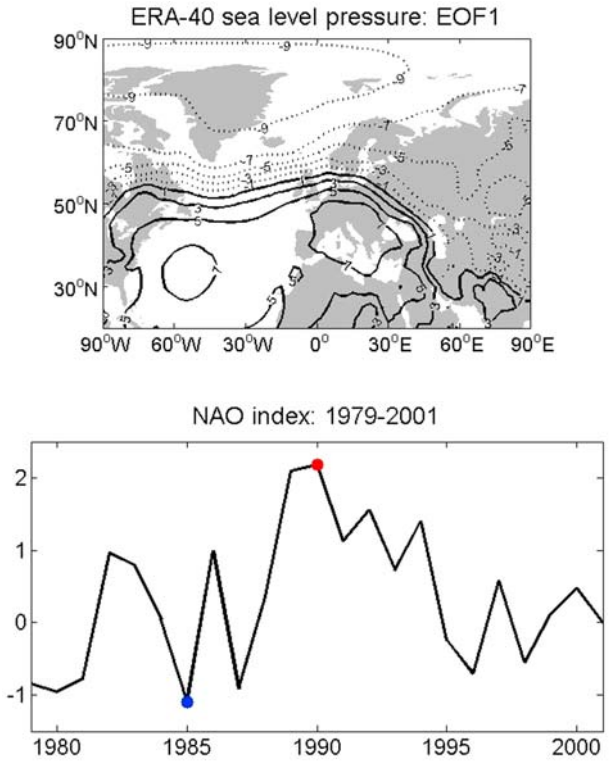

Figure 2. (top) First EOF of ERA-40 annual-mean SLP corresponding to the well known NAO pattern (with the high phase of the NAO pictured here). Negative contours are dashed, and the zero contour is excluded (arbitrary units). (bottom) First EOF time series in units of standard deviations. The blue and red dots correspond to 1985 and 1990, the years of the low and high NAO ROMS simulations.

is the phytoplankton growth rate, l_{BM} and l_E are zooplankton excretion rates, k_p is the half-saturation concentration for phytoplankton ingestion by zooplankton, β is the assimilation efficiency of ingested phytoplankton by zooplankton, r_{SD} and r_{LD} are the remineralization rates of *SDet* and *LDet*, k is a constant, w is the near-surface (10 m) wind speed, Sc is the Schmidt number for CO_2, $CO_{2,sol}$ is the CO_2 solubility, $pCO_{2,air}$ and $pCO_{2,sea}$ are the CO_2 partial pressures of the atmosphere and ocean surface water, $\underline{V}$ is the three-dimensional current velocity vector, and D_{DIC} is the three-dimensional diffusion of DIC within the water column (see *Fennel et al.* [2006, 2008] for a description of the meaning of the different biological parameters in (1) and their prescribed values in ROMS). The first term on the right-hand side of (1) represents the loss of DIC resulting from phytoplankton production of organic matter. Terms 2 and 3 are the zooplankton excretion. The fourth and fifth terms account for the remineralization of *SDet* and *LDet*, respectively. Terms 6 and 7 are the air-sea CO_2 exchange [*Wanninkhof*, 1992], and terms 8 and 9 are the DIC advection and diffusion. DIC is used along with ROMS-predicted SST, sea surface salinity, and total alkalinity (TA) to calculate $pCO_{2,sea}$ using the carbonate chemistry model of *Zeebe and Wolf-Gladrow* [2001]. For $pCO_{2,air}$, we adopt a constant value of 377 ppm, which is the 2004 mean value measured at the Mauna Loa Observatory. TA is affected by phytoplankton uptake of NO_3, nitrification, and advection and diffusion within the water column. Its time rate of change is therefore expressed as

$$\frac{\partial TA}{\partial t} = \mu_{\max} \cdot f(I) \cdot L_{NO3} \cdot Phy - n \cdot NH_4 + \nabla TA \cdot \underline{V} + D_{TA} \quad (2)$$

where $\mu_{\max}$ is the maximum phytoplankton growth rate, *f(I)* describes the photosynthesis-light relationship, L_{NO3} is the Michaelis-Menten function for NO_3, and n is the nitrification rate.

2.2. Experiment Design

[12] ROMS is implemented in the present study over an area that extends from the Scotian Shelf to the Gulf of Mexico and includes the adjacent deep ocean, a region referred to herein as the NorthEast North American (NENA) domain (Figure 1a). The model uses ~10 km horizontal resolution and has 30 terrain-following vertical layers.

[13] To select representative high and low NAO years for the ROMS simulations, we performed an empirical orthogonal function (EOF) analysis on annual-mean sea level pressure (SLP) anomalies over the Northern Hemisphere (NH) Atlantic sector (20°–90°N, 90°W–90°E). SLP fields were taken from the European Centre for Medium-Range Weather Forecasts 40-year reanalysis (ERA-40 [*Uppala et al.*, 2005]), a global data set containing information on the state of the atmosphere, land surface and ocean for the period from September 1957 through August 2002. The first EOF of ERA-40 SLP (Figure 2) explains 37.7% of the year-to-year variance in the data and corresponds to the NAO pattern, which is characterized by SLP anomalies of opposite sign over the Arctic and at midlatitudes. Associated with these SLP anomalies are changes in the strength and position of the surface westerly winds and related changes in storm tracks and precipitation patterns over the NH Atlantic sector (see *Hurrell et al.* [2003] for a summary of NAO-related climate effects in this region). The NAO has also been linked to recent changes in oceanic CO_2 uptake in the North Atlantic [*Thomas et al.*, 2008]. Using the first EOF time series (Figure 2) as an index for the NAO pattern, we selected the years with the lowest and highest NAO indices (1985 and 1990, respectively) for our ROMS simulations, employing ERA-40 atmospheric fields for these years to force the model. Acquired ERA-40 fields include SLP, surface downwelling longwave radiation, surface net shortwave radiation, 2 m air temperature and relative humidity, 10 m u and v wind components, and surface precipitation rate. Fields were obtained at 6 h intervals, but were averaged to daily resolution to force ROMS.

[14] Both the high and low NAO model simulations were initialized on 1 January using ROMS output from a previously completed run over the NENA domain [*Fennel et al.*, 2008]. Open boundary temperatures, salinities and transports from the Hybrid Coordinate Ocean Model (HyCOM [*Chassignet et al.*, 2007]) were prescribed after first removing known biases in HyCOM temperatures and salinities [*Fennel et al.*, 2008]. HyCOM open boundary transports were augmented with barotropic tides from the global analysis of *Egbert and Erofeeva* [2002]. Monthly climatological freshwater input from rivers was specified based on observed freshwater fluxes at U.S. Geological Survey–

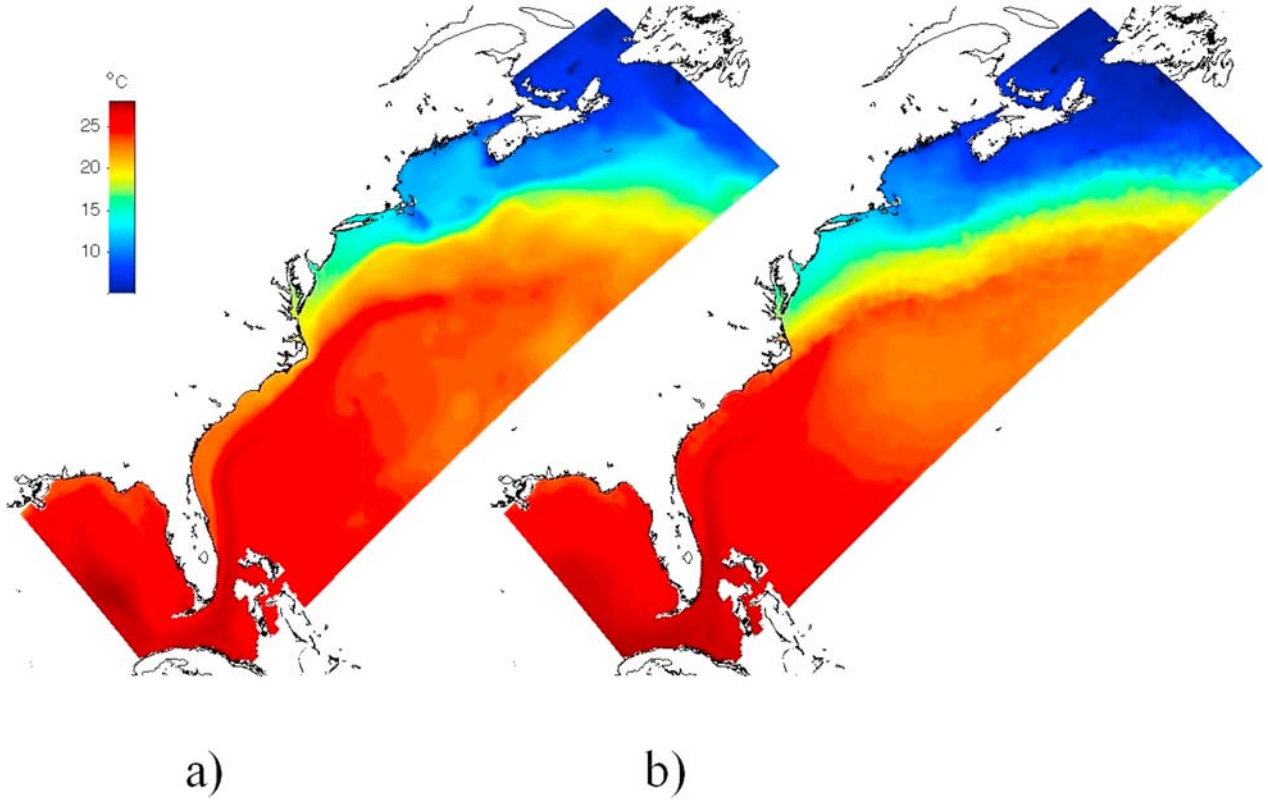

Figure 3. Annual-mean SST (averaged for the years 1985 and 1990) from (a) ROMS and (b) AVHRR.

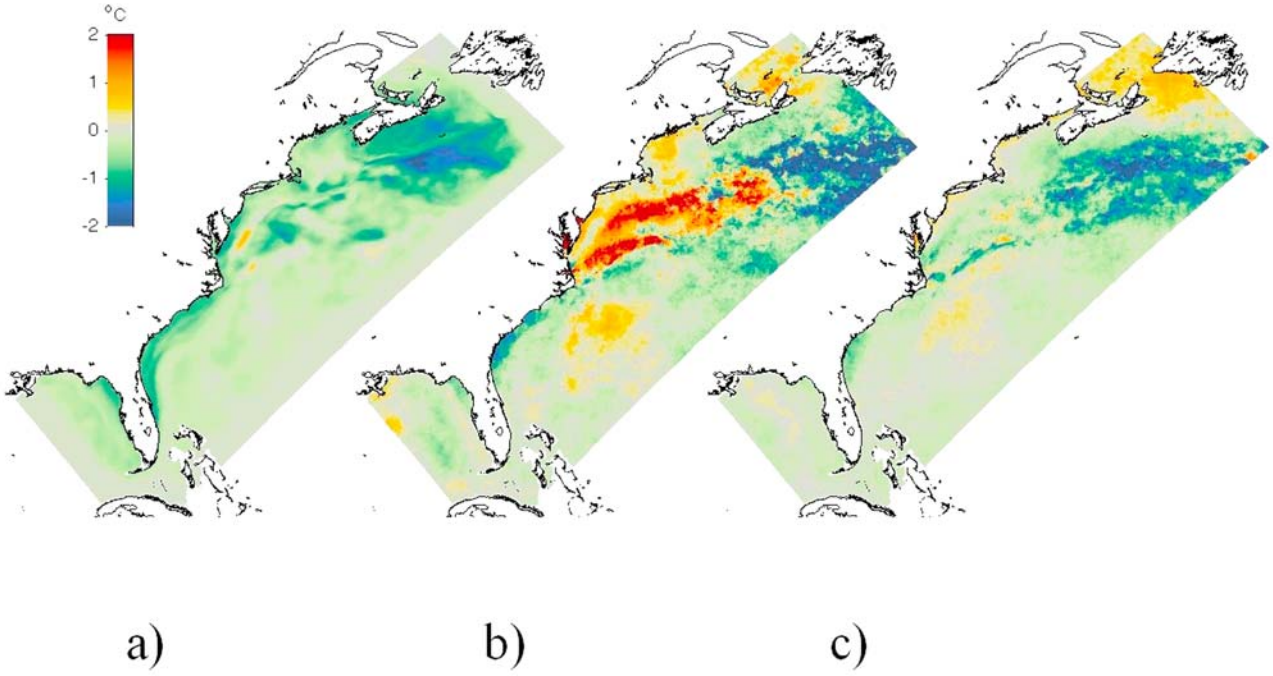

Figure 4. Difference in annual-mean SST (1985–1990) in (a) ROMS and (b) AVHRR. (c) The observed anomalous SST field during the low phase of the NAO based on an average of 4 low NAO (1985, 1987, 1996, 1998) and 4 high NAO (1989, 1990, 1992, 1994) years.

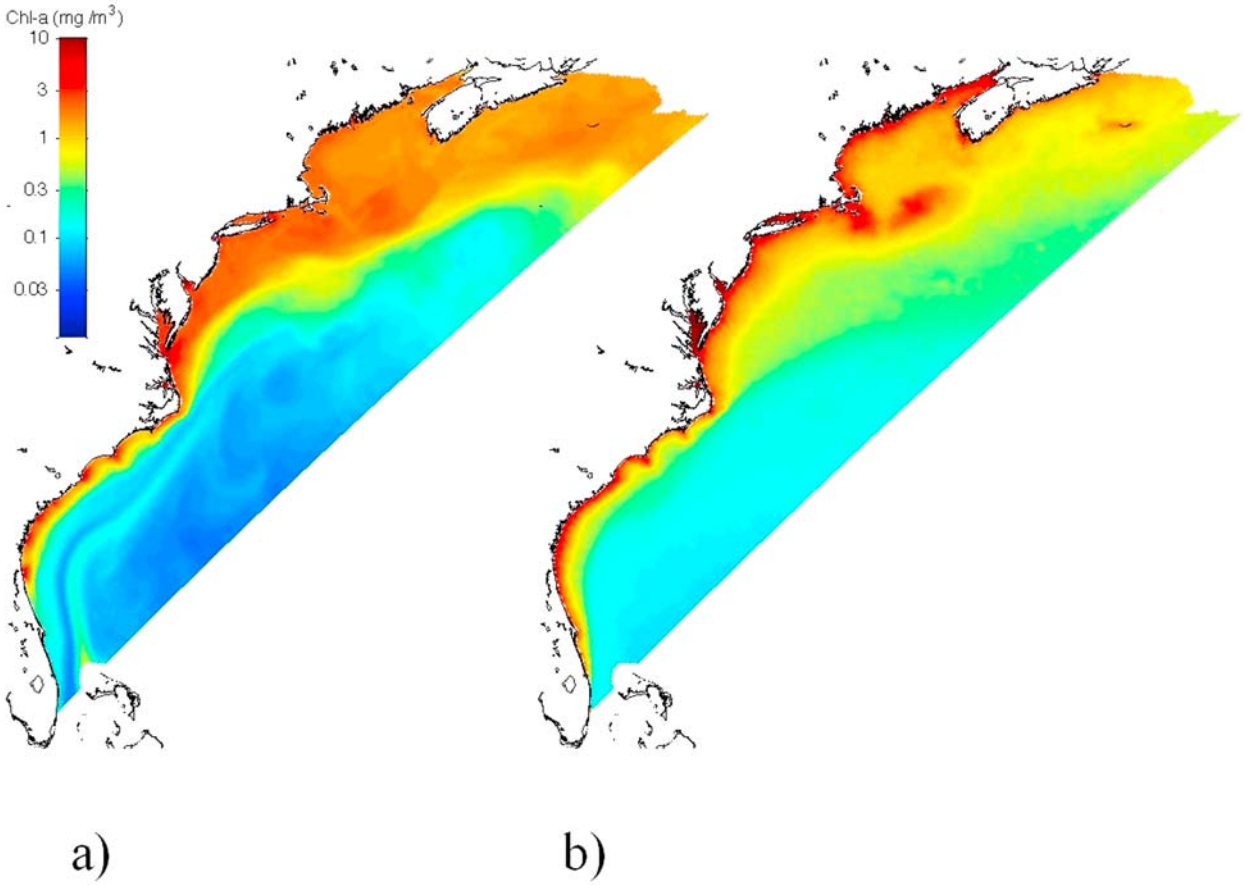

Figure 5. Annual-mean surface chlorophyll concentration based on (a) ROMS output averaged for 1985 and 1990 and (b) SeaWiFS climatology.

gauged rivers. Riverine nitrogen concentrations were determined from the watershed analysis of *Dumont et al.* [2005], while TA in rivers was prescribed using *Millero et al.*'s [1998] relationship for a salinity of zero. DIC concentrations in rivers were assumed to be in equilibrium with $pCO_{2,air}$. The assumed river TA and DIC concentrations may not necessarily be realistic; for example, highly productive estuaries in the SAB often discharge supersaturated water [*Cai et al.*, 2003], but undersaturated discharge is observed as well with significant temporal and interestuary variability [*Salisbury et al.*, 2008]. However, detailed and continuous DIC and TA data are not available at present for the 32 rivers included in our model.

3. Model-Data Comparison

[15] In this section, ROMS output is evaluated using available observations [see also *Fennel et al.*, 2008]. We initially focus on the entire NENA domain, and then assess model skill in more detail for the northeast U.S. continental shelf.

[16] Figure 3 shows the annual-mean SST (averaged for the years 1985 and 1990) as simulated by ROMS and as observed by the AVHRR satellite. ROMS generally reproduces the satellite-measured SST pattern, although warm water associated with the Gulf Stream extends slightly too far to the north and west in the model, resulting in positive SST biases of $\sim$2–3°C in portions of the MAB and MAB slope sea. The model is also too warm in the GOM by about the same amount. In Figures 4a and 4b, the SST difference (1985–1990) in ROMS and AVHRR is shown. The model captures the observed negative SST anomalies over a broad area southeast of the Scotian Shelf, over portions of the northeast Gulf of Mexico, and over the SAB. Not present in the model results, however, is the area of positive SST anomalies in AVHRR over the MAB slope sea and adjacent deep ocean. In Figure 4c, we plot the observed anomalous SST field during the low phase of the NAO based on an average of 4 low NAO (1985, 1987, 1996, 1998) and 4 high NAO (1989, 1990, 1992, 1994) years. (These 8 years represent the most extreme years in the NAO index (Figure 2) since the start of the AVHRR record in late 1981.) The aforementioned negative SST anomalies are still evident, while the area of positive SST anomalies in Figure 4b is not. This suggests that the latter is not a robust SST response to NAO variability, and we therefore conclude that ROMS is successful in simulating the main features of this response.

[17] Figure 5 compares annual-mean surface chlorophyll concentrations in ROMS and SeaWiFS. The model reproduces the general pattern of enhanced productivity in coastal zones and diminished productivity over the open ocean, and also captures specific features seen in the SeaWiFS data such as the elevated chlorophyll concentra-

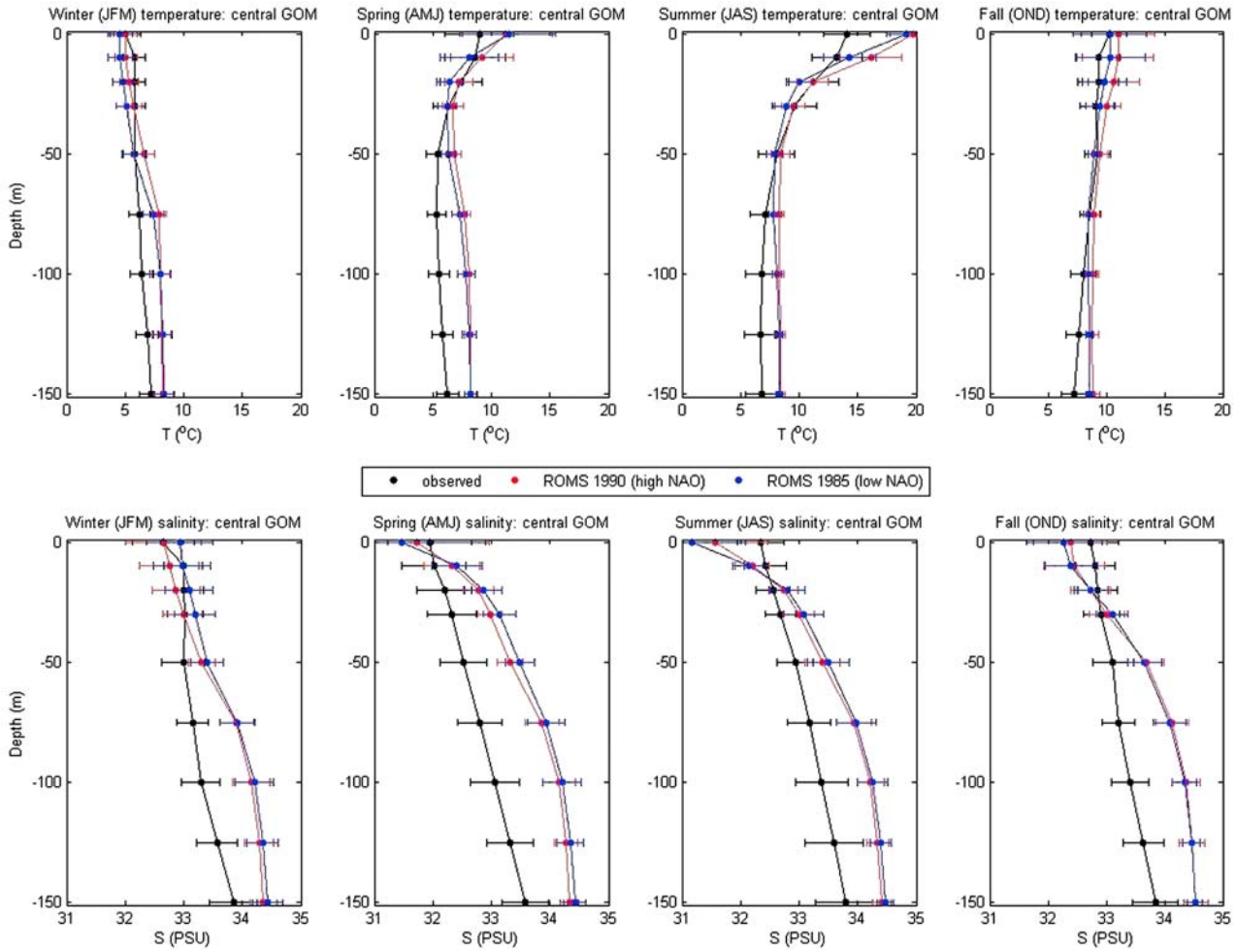

Figure 6. Modeled and observed climatological seasonal temperature and salinity profiles for the central GOM. Error bars correspond to the ±1-sigma levels.

tions over Georges Bank. The model underestimates satellite-derived chlorophyll in the most nearshore regions; however, algorithms estimating chlorophyll from ocean color (such as are used by SeaWiFS) are known to be problematic for the optically complex nearshore waters and may overestimate true chlorophyll concentrations.

[18] We now assess model skill over the northeast U.S. continental shelf in more detail by comparing ROMS results with observations for the MAB/GOM subregions shown in Figure 1b. Figures 6 and 7 depict seasonal temperature/salinity and NO_3/chlorophyll profiles for the central GOM. Similar plots for the other 5 subregions are provided in Figures S1–S10 (available as auxiliary material).[1] (Additionally, various statistical measures of model-data agreement are summarized in Table 1 for the central GOM and in Tables S1–S5 for the other subregions. For reference, modeled DIC/TA profiles are shown in Figures S11–S16, even though observational data for these fields were not available for comparison.) The observational data used to generate Figures 6 and 7 and Figures S1–S10 were acquired from the National Oceanographic Data Center (NODC) World Ocean Database 2005 (http://www.nodc.noaa.gov/OC5/WOD05/pr_wod05.html). NODC data were supplemented with additional in situ NO_3 and chlorophyll data from the Ocean Margins Program in 1994 (OMP [*Verity et al.*, 2002]), the Shelf Edge Exchange Processes (SEEP) programs in 1983–1984 and 1988–1989 [*Walsh et al.*, 1988; *Biscaye et al.*, 1994], a number of cruises undertaken by Brookhaven National Laboratory between 1974 and 1995 (BNL data reports), and the MARMAP cruises between 1977 and 1988 [*O'Reilly and Zetlin*, 1998]. NODC data were acquired on standard depth levels, and all other observational and model data were linearly interpolated to these levels. It is evident from Figure 6 that the simulated positive annual-mean SST biases in the GOM noted earlier arise mainly as a result of the model being too warm in the summertime. Below the surface, modeled temperatures are close to those observed, indicating that the seasonal thermocline is too sharp in ROMS. The model tends to be too fresh at the surface and too salty at depth in the central GOM. ROMS NO_3 concentrations generally fall within the error bars of the observations except for at depths greater than 50 m in the fall (Figure 7). Observed NO_3 amounts are similarly under-

[1] Auxiliary materials are available in the HTML. doi:10.1029/2008JG000881.

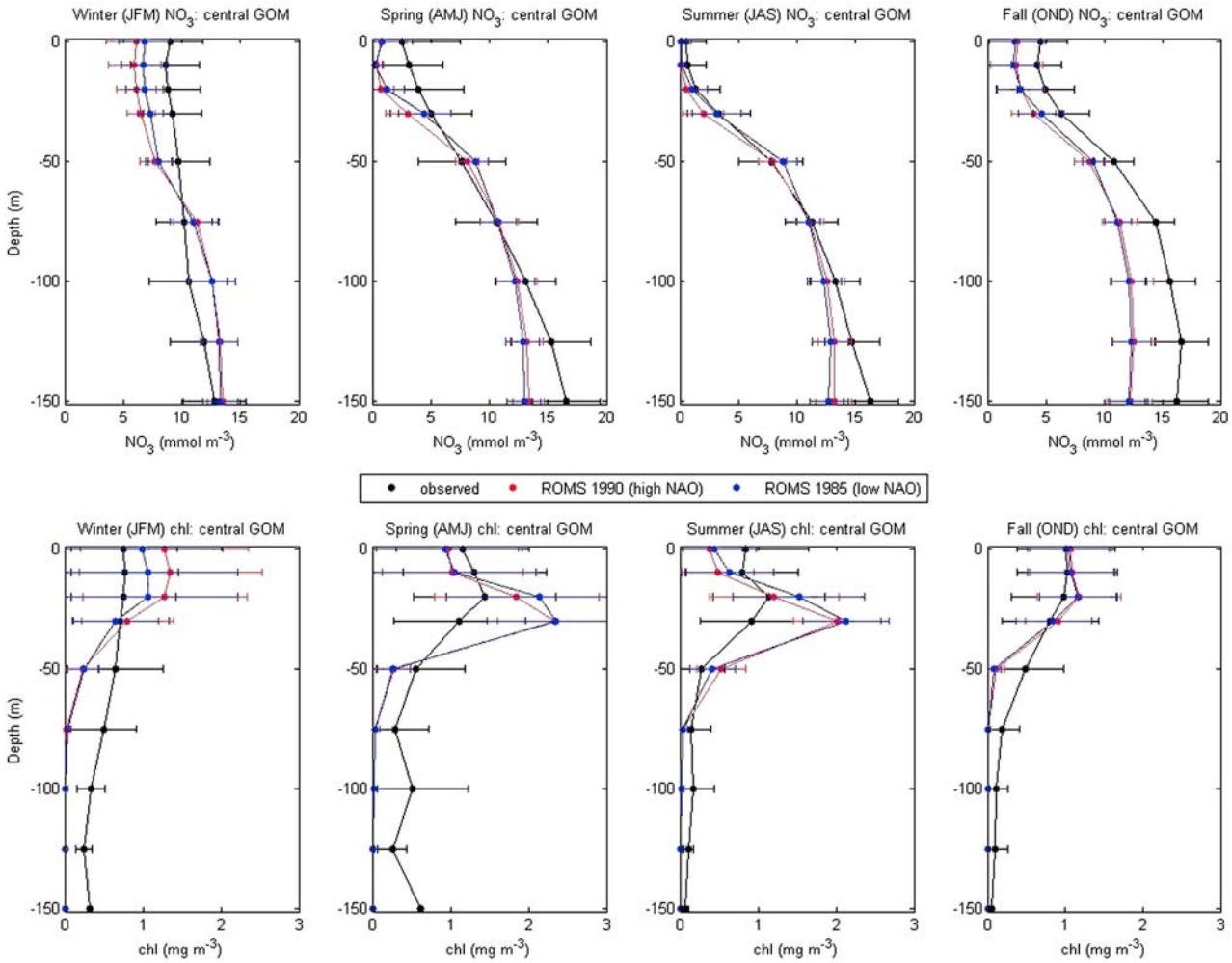

Figure 7. As in Figure 6, but for NO_3 and chlorophyll.

estimated at depth in the outer MAB and MAB slope sea (Figures S4 and S6). ROMS chlorophyll amounts are generally within the error bars of the observations in all subregions. The model captures the observed subsurface chlorophyll maximum in the spring and summer in the outer MAB, MAB slope sea and central GOM (Figures S4, S6, and 7).

[19] Overall, ROMS reproduces the observed spatial and seasonal variability of temperature, salinity, NO_3 and chlorophyll with a relatively high level of skill. At the surface where the air-sea exchange of CO_2 occurs, simulated and observed fields agree within one standard deviation in all cases except for the summer temperature in the central GOM (Figure 6) and the summer and fall salinity on Georges Bank (Figure S7). We show in the next section that modeled estimates of the annual air-sea flux of CO_2 are also consistent with available observations.

4. Simulated CO_2 Air-Sea Flux and Its Interannual Variability

[20] The modeled annually integrated CO_2 air-sea flux F for the northeast U.S. continental shelf is shown in Figure 8. During both 1985 (low NAO) and 1990 (high NAO), F is positive over most of the shelf, indicating a net uptake of atmospheric CO_2 by the ocean. The strongest uptake occurs in the GOM during both years and in the northern half of the MAB during 1985 (Figure 8a). Localized areas of net annual CO_2 outgassing from the ocean (negative F) are evident over the inner MAB (e.g., off the Delmarva Peninsula). Over the northeast U.S. shelf as a whole, the total atmospheric CO_2 uptake is 2.4 Mt C yr^{-1} during 1985, with 1.1 Mt C yr^{-1} of this uptake occurring in the MAB and the remaining 1.3 Mt C yr^{-1} occurring in the GOM. During 1990, CO_2 uptake on the northeast shelf is reduced to 1.8 Mt C yr^{-1} (0.6 and 1.2 Mt C yr^{-1} in the MAB and GOM, respectively). *DeGrandpre et al.* [2002] used observed $pCO_{2,sea}$ values to estimate a total annual CO_2 uptake on the MAB of 1.6±1 Mt C yr^{-1}, which encompasses the 1.1 and 0.6 Mt C yr^{-1} modeled estimates of F reported here. (Following *Fennel et al.* [2008], we recalculated DeGrandpre et al.'s total CO_2 flux using areal sizes of 3.15×10^{10}, 4.80×10^{10} and 4.54×10^{10} m^2 for the inner, mid and outer MAB.) *Fennel et al.* [2008] found a slightly larger MAB CO_2 uptake of 1.7 Mt C yr^{-1}. The difference in F between 1985 and 1990 is shown in Figure 9a. The largest positive differences occur over the northern and central MAB, with smaller positive F differences in the coastal

Table 1. Temperature, Salinity, NO_3, and Chlorophyll Statistics for the Central GOM[a]

Depth (m)	Observed Mean	Average Bias	RMSE	Observed σ	ROMS σ
		Temperature (°C)			
0	9.60	1.97	2.93	3.73	6.02
10	9.24	0.601	1.30	3.07	4.34
20	8.44	−0.251	0.725	2.34	2.69
30	7.75	−0.0386	0.424	1.94	2.11
50	7.12	0.406	0.618	1.83	1.41
75	6.81	1.17	1.40	1.41	0.539
100	6.70	1.52	1.66	1.04	0.298
125	6.77	1.56	1.63	0.746	0.231
150	6.90	1.50	1.54	0.475	0.207
		Salinity (PSU)			
0	32.4	−0.391	0.556	0.355	0.657
10	32.6	−0.109	0.298	0.433	0.294
20	32.7	0.172	0.339	0.358	0.111
30	32.7	0.323	0.412	0.306	0.0233
50	32.9	0.574	0.605	0.256	0.140
75	33.1	0.887	0.898	0.193	0.100
100	33.3	0.954	0.960	0.162	0.0819
125	33.5	0.838	0.844	0.147	0.0719
150	33.8	0.667	0.673	0.127	0.0656
		NO_3 (mmol m^{-3})			
0	4.17	−1.70	1.86	3.60	2.87
10	4.13	−1.84	2.02	3.33	2.89
20	4.77	−1.99	2.18	3.11	2.62
30	5.99	−1.60	1.72	2.49	1.83
50	9.01	−0.594	1.45	1.58	0.406
75	11.6	−0.577	1.67	1.92	0.203
100	13.2	−0.754	2.08	2.10	0.159
125	14.6	−1.68	2.61	2.01	0.337
150	15.5	−2.58	3.17	1.80	0.524
		Chlorophyll (mg m^{-3})			
0	0.941	−0.0542	0.307	0.176	0.330
10	0.977	−0.0043	0.285	0.251	0.283
20	1.08	0.348	0.381	0.286	0.389
30	0.889	0.618	0.844	0.173	0.820
50	0.492	−0.224	0.332	0.156	0.156
75	0.281	−0.252	0.286	0.158	0.0111
100	0.281	−0.268	0.309	0.181	0.00480
125	0.179	−0.174	0.188	0.0842	0.00180
150	0.263	−0.260	0.349	0.269	0.000800

[a]Shown for each field are the observed annual mean, average bias (ROMS minus observed), root mean square error (RMSE), and observed and simulated interseasonal standard deviation.

GOM. Negative F differences (denoting reduced atmospheric CO_2 uptake during 1985) are apparent over portions of the southern MAB and central GOM.

4.1. Method

[21] The air-sea flux of CO_2 depends on Sc, $CO_{2,sol}$, w and $pCO_{2,sea}$ (see terms 6 and 7 in equation (1)). Here we examine the contributions of these variables to the interannual change in F. We approximate the difference δF in the annually integrated CO_2 flux using a second-order Taylor series expansion:

$$\delta F \approx \sum_{i=1}^{n} \frac{\partial F}{\partial X_i}\delta X_i + \frac{1}{2}\sum_{i=1}^{n}\sum_{j=1}^{n}\frac{\partial^2 F}{\partial X_i \partial X_j}\delta X_i \delta X_j \qquad (3)$$

where $X = (X_1, \ldots, X_n)$ are variables in the equation for F (i.e., $F = F(X_1, \ldots, X_n) = F(Sc, CO_{2,sol}, w, pCO_{2,sea})$). A similar method was employed by *Colman et al.* [1997] to estimate radiative feedbacks in an atmospheric general circulation model. First-order partial derivatives in (3) are approximated using a method of single field substitution, i.e.,

$$\frac{\partial F}{\partial X_i}\delta X_i \approx F\left(\underline{X}^{1990} + \underline{e}_i \Delta \underline{X}\right) - F\left(\underline{X}^{1990}\right) \qquad (4)$$

where $\Delta \underline{X} = \underline{X}^{1985} - \underline{X}^{1990}$ and $\underline{e}_i$ is the ith unit vector.

[22] To compute the first term on the right-hand side of (4), we calculated the CO_2 air-sea flux using the time series of variable X_i from the 1985 ROMS simulation and the time series of all other variables from the 1990 simulation, and then integrated over the entire year. The second term on the right-hand side of (4) was computed using the time series of all variables from the 1990 model simulation. This method of single field substitution was used by *Wetherald and Manabe* [1988] to diagnose cloud radiative feedbacks in a global climate model. It provides estimates of the linear sensitivity of F to various changes in the air-sea system (i.e., the change in F due to a change in Sc, $CO_{2,sol}$, w, or $pCO_{2,sea}$ alone). Nonlinear effects contributing to δF are estimated by computing the second-order partial derivatives in (3). These higher-order derivatives are approximated as

$$\begin{aligned}\frac{\partial^2 F}{\partial X_i \partial X_j}\delta X_i \delta X_j \approx & \left(F\left(\underline{X}^{1990} + \left(\underline{e}_i + \underline{e}_j\right)\Delta \underline{X}\right) - F\left(\underline{X}^{1990} + \underline{e}_j \Delta \underline{X}\right)\right) \\ & - \left(F\left(\underline{X}^{1990} + \underline{e}_i \Delta \underline{X}\right) - F\left(\underline{X}^{1990}\right)\right) \\ = & \left(F\left(\underline{X}^{1990} + \left(\underline{e}_i + \underline{e}_j\right)\Delta \underline{X}\right) - F\left(\underline{X}^{1990} + \underline{e}_j \Delta \underline{X}\right)\right) \\ & - \frac{\partial F}{\partial X_i}\delta X_i \end{aligned} \qquad (5)$$

where $F(X^{1990} + (e_i + e_j)\Delta X)$ was calculated using the time series of X_i and X_j from the 1985 ROMS simulation and the time series of all other variables from the 1990 simulation. (5) provides an indication of how the sensitivity of F to changes in X_i depends on X_j, or, more generally, of how this sensitivity depends on the state of the system.

4.2. Results

[23] The difference in air-sea CO_2 flux between 1985 and 1990, δF, is shown in comparison with its second-order Taylor series approximation in Figures 9a and 9b. (The first-order Taylor series approximation is very similar (not shown).) Comparison of Figures 9a and 9b indicates that δF is reproduced almost exactly (mean absolute difference of 1.9 mmol C m^{-2} yr^{-1} between Figures 9a and 9b). Contributions of Sc and $CO_{2,sol}$ changes to δF are small and nearly cancel one another (not shown), implying that the CO_2 flux difference between 1985 and 1990 is due to changes in w and/or $pCO_{2,sea}$. Figure 9c shows the w contribution to δF (i.e., the sum of the first- and second-order partial derivatives of F with respect to w in (3)). Interannual differences in w between 1985 and 1990 act to increase atmospheric CO_2 uptake during the former year over nearly all of the MAB, while having a relatively small effect on F over most of the GOM. The enhanced CO_2 uptake over the northern half of the MAB in Figures 9a and 9b is a response primarily to w changes. Higher near-surface wind speeds will enhance atmospheric CO_2 uptake by the ocean at times of year when the surface water is undersaturated with respect to $pCO_{2,air}$, but will have the opposite effect on F

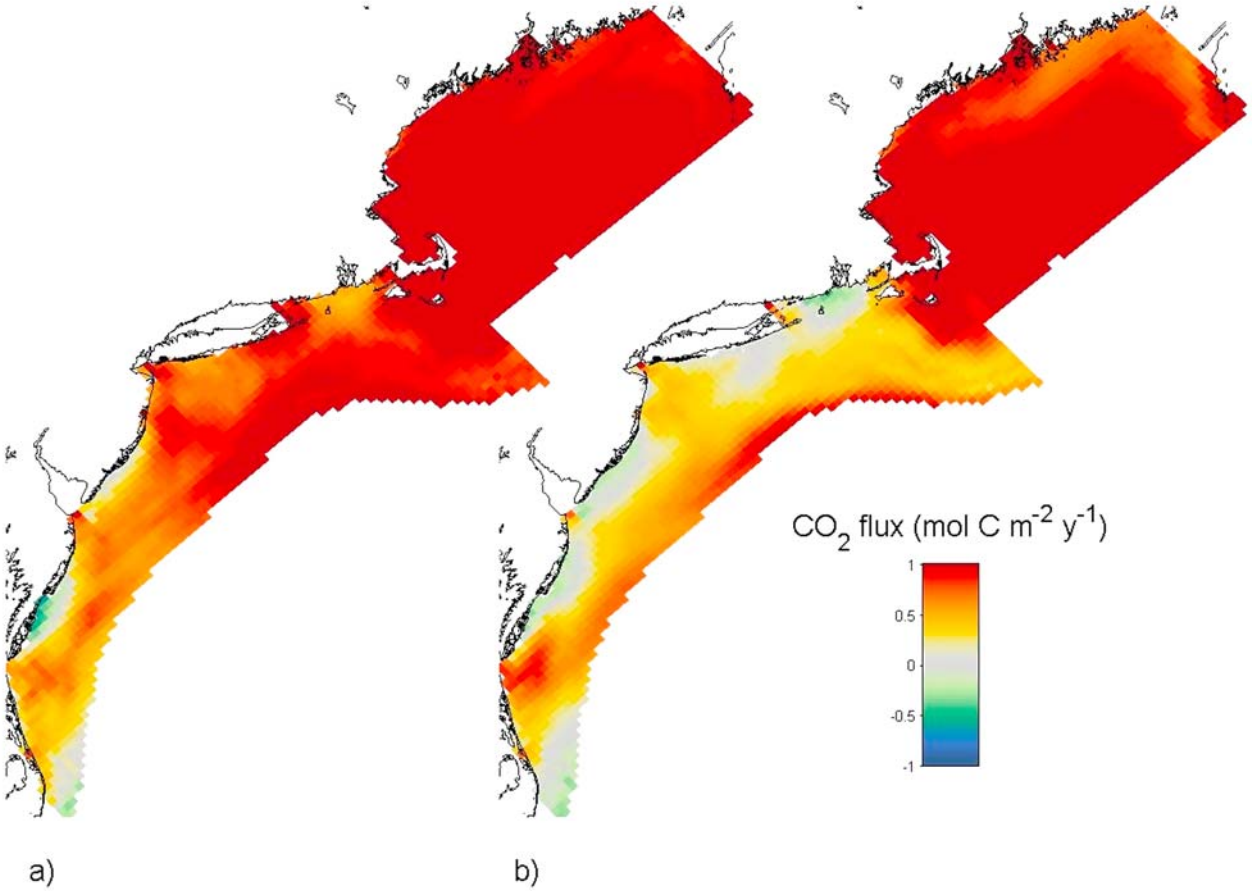

Figure 8. ROMS simulated annually integrated CO_2 air-sea flux for the northeast U.S. continental shelf for (a) 1985 (low NAO) and (b) 1990 (high NAO). Positive values denote flux into the ocean.

when the ocean is supersaturated with respect to atmospheric CO_2 levels. In the MAB, the surface ocean is undersaturated in the winter and supersaturated in the summer [e.g., *DeGrandpre et al.*, 2002]. Figure 9c shows the difference (1985–1990) in wintertime (JFM) mean w plotted as black contours. Wind speeds are higher during JFM 1985 over all of the MAB (particularly in the north), thus enhancing atmospheric CO_2 uptake during these months. Conversely, wind speeds are lower in the summer of 1985 than in the summer of 1990 over the northern MAB (not shown), which further contributes to the anomalous uptake of CO_2 during the former year in this region. Finally, in Figure 9d, the contribution of $pCO_{2,sea}$ (hereafter simply pCO_2) changes to δF is shown. Negative contributions to δF over portions of the southern MAB outweigh the positive contributions from w changes in these areas, resulting in a net decrease in atmospheric CO_2 uptake during 1985 (Figures 9a and 9b). The δF pattern in the GOM arises primarily due to pCO_2 changes.

[24] To further understand the pCO_2 changes that contribute to δF, we used the Taylor series method described in section 4.1 to decompose the difference in annual-mean pCO_2 between 1985 and 1990 (Figure 10a). Figures 10b and 10c show the first and second-order Taylor series approximations to the pCO_2 difference. While the first-order approximation is poor, the second-order approximation closely matches the actual difference in pCO_2 (mean absolute difference of 1.8 ppm between Figures 10a and 10c). (The poor first-order approximation to the pCO_2 difference will be discussed more below.) Figure 10c is the sum of Figures 10d–10g, which represent, respectively, the pCO_2 differences due to interannual differences in SST, sea surface salinity, biological activity, and mixing/CO_2 air-sea gas exchange. (In this case, mixing refers to the advection and diffusion of water masses with different DIC/TA characteristics.) Lower SSTs in 1985 relative to 1990 act to decrease pCO_2 (and thus increase the uptake of atmospheric CO_2) over nearly all of the northeast U.S. continental shelf. The negative pCO_2 anomalies over the coastal GOM (Figures 10a and 10c) are clearly a response in part to these SST changes. By comparison the effects of salinity on the difference in annual-mean pCO_2 (Figure 10e) are small, although increases in salinity during 1985 partially explain the positive pCO_2 anomalies over the outer MAB. Figure 10f shows pCO_2 changes owing to the biological contribution. This contribution represents the effects of anomalous biological activity on DIC and TA (i.e., the effects of interannual differences in terms 1–5 in equation (1) and in terms 1–2 in equation (2)). Overlaid as black contours in Figure 10f is the difference in the average rate of net ecosystem production NEP (i.e., net primary production minus respiration) between 1985 and 1990. Areas of enhanced NEP (e.g., the coastal GOM) are associated with a negative biological contribution to the

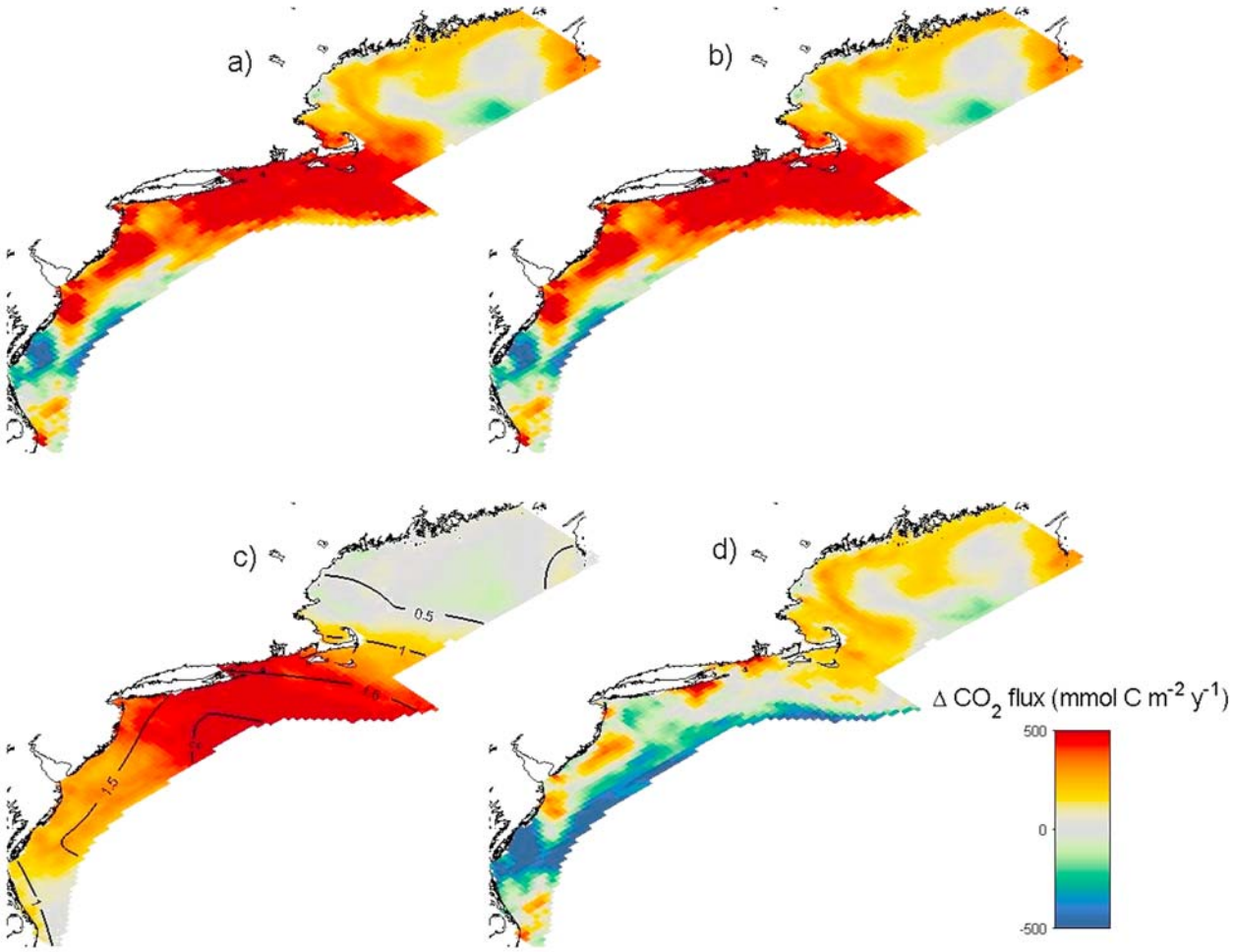

Figure 9. (a) Difference in annually integrated CO_2 air-sea flux (1985 minus 1990). (b) Second-order Taylor series approximation to Figure 9a. (c) CO_2 flux difference attributable to near-surface (10 m) wind speed changes. The actual wind speed difference (1985–1990) for winter (JFM) is shown with black contours (contour interval of 0.5 m s^{-1}). (d) CO_2 flux difference due to $pCO_{2,sea}$ changes.

annual-mean pCO_2 difference, while reduced NEP areas (the central GOM and most of the MAB) are those where the biological contribution to pCO_2 is positive. The effects of anomalous biological activity on pCO_2 are largely offset by the effects of anomalous mixing/CO_2 air-sea gas exchange (Figure 10g). Increased biological production of organic matter, for example, will draw down surface water DIC and pCO_2, promoting an increase in atmospheric CO_2 uptake which will counter the effects of enhanced production. Alternatively, stronger biological NO_3 uptake will increase TA and decrease pCO_2. This anomalous NO_3 uptake, however, will tend to be accompanied by anomalous diffusion of high TA water out of the surface layer, again opposing the biological effect. The net effect of interannual changes in biology and mixing/CO_2 air-sea flux on pCO_2 is shown in Figure 10h.

[25] The poor first-order Taylor series approximation to the annual-mean difference in pCO_2 (Figure 10b) indicates that the effect of different processes (e.g., NEP, air-sea gas exchange) on pCO_2 depends on the state of the system. For example, a given magnitude CO_2 flux from the atmosphere to the ocean will produce a larger increase in pCO_2 at lower surface water pH. This is because at lower pH there is less carbonate available to react with the CO_2, and thus more CO_2 will remain dissolved in the surface water. The effect of this is to reduce the CO_2 uptake from the atmosphere, and this mechanism is expected to significantly diminish the ocean's capacity to absorb anthropogenic CO_2 in the future.

5. Summary and Conclusions

[26] The current work represents the first systematic modeling study of interannual (NAO-related) variability in atmospheric CO_2 uptake on the northeast U.S. continental shelf. ROMS simulated CO_2 uptake on the northeast shelf was found to decrease from 2.4 Mt C yr^{-1} in 1985 (low NAO) to 1.8 Mt C yr^{-1} in 1990 (high NAO), with most of this decrease (0.5 Mt C yr^{-1}) occurring in the MAB. The magnitude of interannual variation in the CO_2 air-sea flux on the northeast U.S. shelf may be even larger than estimated here. For example, *Fennel et al.* [2008] found an MAB CO_2 uptake of 1.7 Mt C yr^{-1}, larger than the 1.1 and 0.6 Mt C yr^{-1} uptakes simulated in the present study. These results suggest that the CO_2 air-sea flux on the MAB

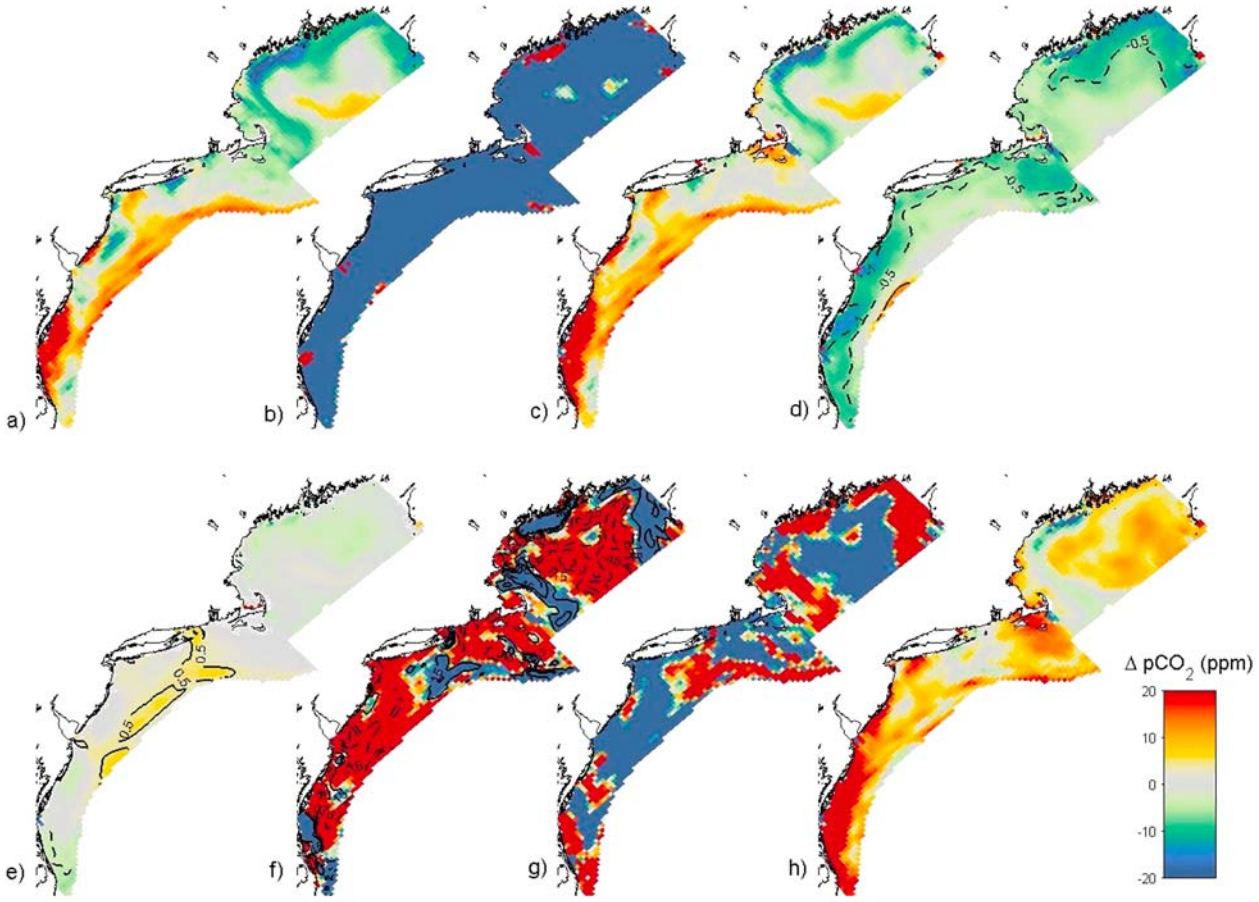

Figure 10. (a) Difference in annual-mean $pCO_{2,sea}$ (1985–1990). (b) First-order Taylor series approximation to Figure 10a. (c) Second-order Taylor series approximation to Figure 10a. (d) The $pCO_{2,sea}$ difference due to SST changes. The actual annual-mean SST difference is overlaid as black contours (contour interval of 0.5°C with negative contours dashed and the zero contour excluded). (e) As in Figure 10d, but for changes in $pCO_{2,sea}$ attributable to sea surface salinity. Black contours show the annual-mean salinity difference in PSU. (f) The $pCO_{2,sea}$ difference due to biology changes. Black contours show the 1985–1990 difference in the average rate of net ecosystem production at the surface (contour interval of 15 mmol C m^{-2} yr^{-1} with negative contours dashed and the zero contour excluded). (g) The $pCO_{2,sea}$ difference due to DIC/TA mixing and CO_2 air-sea flux changes. (h) Sum of Figures 10f and 10g.

may vary by a factor of 2–3 from one year to the next. In other continental shelf systems, interannual variability might be even greater. For instance, as noted in section 1, *Arrigo and Van Dijken* [2007] estimated that atmospheric CO_2 uptake by the Ross Sea, Antarctica varies more than twentyfold between years, largely as a result of interannual changes in sea ice cover. Accounting for such potentially large interannual variability is important when attempting to quantify the role of continental shelf systems globally in the air-sea exchange of CO_2.

[27] We used a novel technique (a second-order Taylor series decomposition) to identify the important processes responsible for producing year-to-year changes in the CO_2 air-sea flux. Different processes were found to be important in different regions. In the MAB, most of the increased CO_2 uptake during 1985 relative to 1990 was found to be due to changes in near-surface wind speed, while in the GOM CO_2 flux differences were primarily controlled by surface ocean pCO_2 variations resulting from changes in SST and NEP. Future changes in the air-sea exchange of CO_2 associated with anthropogenic climate change will involve a similarly complex interaction of many processes. It is important to point out that the magnitude of interannual climate change considered in the present study is small compared to the changes that are anticipated to occur throughout the remainder of the current century. For example, annual-mean SST differences between 1985 and 1990 on the northeast U.S. continental shelf are at most ~1°C (e.g., see Figure 10d). By contrast, global climate models predict that annual-mean surface air temperature in this region will increase by about 2.5–3°C by the end of the 21st century under the A1B emission scenario [*Meehl et al.*, 2007]. Thus, if variations in the air-sea exchange of CO_2 scale with the magnitude of the climate change, then significantly larger changes in atmospheric CO_2 uptake on the northeast U.S. shelf can be expected in the future.

[28] **Acknowledgments.** We thank an anonymous reviewer whose comments helped strengthen the manuscript. Katja Fennel acknowledges support from NSERC, CFI, and the CRC program.

References

Arrigo, K. R., and G. L. Van Dijken (2007), Interannual variation in air-sea CO_2 flux in the Ross Sea, Antarctica: A model analysis, *J. Geophys. Res.*, *112*, C03020, doi:10.1029/2006JC003492.

Bindoff, N. L., et al. (2007), Observations: Oceanic climate change and sea level, in *Climate Change 2007: The Physical Science Basis. Contribution of Working Group I to the Fourth Assessment Report of the Intergovernmental Panel on Climate Change*, edited by S. Solomon et al., Cambridge Univ. Press, New York.

Biscaye, P. E., C. N. Flagg, and P. G. Falkowski (1994), The Shelf Edge Exchange Processes experiment, SEEP-II: An introduction to hypotheses, results and conclusions, *Deep Sea Res., Part II*, *41*, 231–252, doi:10.1016/0967-0645(94)90022-1.

Borges, A. V., B. Delille, and M. Frankignoulle (2005), Budgeting sinks and sources of CO_2 in the coastal ocean: Diversity of ecosystems counts, *Geophys. Res. Lett.*, *32*, L14601, doi:10.1029/2005GL023053.

Cai, W.-J., Z. A. Wang, and Y. Wang (2003), The role of marsh-dominated heterotrophic continental margins in transport of CO_2 between the atmosphere, the land-sea interface and the ocean, *Geophys. Res. Lett.*, *30*(16), 1849, doi:10.1029/2003GL017633.

Cai, W.-J., M. Dai, and Y. Wang (2006), Air-sea exchange of carbon dioxide in ocean margins: A province-based synthesis, *Geophys. Res. Lett.*, *33*, L12603, doi:10.1029/2006GL026219.

Chassignet, E. P., H. E. Hurlburt, O. M. Smedstad, G. R. Halliwell, P. J. Hogan, A. J. Wallcraft, R. Baraille, and R. Bleck (2007), The HYCOM (HYbrid Coordinate Ocean Model) data assimilative system, *J. Mar. Syst.*, *65*, 60–83, doi:10.1016/j.jmarsys.2005.09.016.

Colman, R. A., S. B. Power, and B. J. McAvaney (1997), Non-linear climate feedback analysis in an atmospheric general circulation model, *Clim. Dyn.*, *13*, 717–731, doi:10.1007/s003820050193.

DeGrandpre, M. D., G. J. Olbu, C. M. Beatty, and T. R. Hammar (2002), Air-sea CO_2 fluxes on the US Middle Atlantic Bight, *Deep Sea Res., Part II*, *49*, 4355–4367, doi:10.1016/S0967-0645(02)00122-4.

Dumont, E., J. A. Harrison, C. Kroeze, E. J. Bakker, and S. P. Seitzinger (2005), Global distribution and sources of dissolved inorganic nitrogen export to the coastal zone: Results from a spatially explicit, global model, *Global Biogeochem. Cycles*, *19*, GB4S02, doi:10.1029/2005GB002488.

Egbert, G. D., and S. Y. Erofeeva (2002), Efficient inverse modeling of barotropic ocean tides, *J. Atmos. Oceanic Technol.*, *19*, 183–204, doi:10.1175/1520-0426(2002)019<0183:EIMOBO>2.0.CO;2.

Fairall, C. W., E. F. Bradley, J. E. Hare, A. A. Grachev, and J. Edson (2003), Bulk parameterization of air–sea fluxes: Updates and verification for the COARE algorithm, *J. Clim.*, *16*, 571–591, doi:10.1175/1520-0442(2003)016<0571:BPOASF>2.0.CO;2.

Fasham, M. J. R., H. W. Ducklow, and S. M. McKelvie (1990), A nitrogen-based model of plankton dynamics in the oceanic mixed layer, *J. Mar. Res.*, *48*, 591–639.

Feely, R. A., C. L. Sabine, J. M. Hernandez-Ayon, D. Ianson, and B. Hales (2008), Evidence for upwelling of corrosive "acidified" water onto the continental shelf, *Science*, *320*, 1490–1492, doi:10.1126/science.1155676.

Fennel, K., J. Wilkin, J. Levin, J. Moisan, J. O'Reilly, and D. Haidvogel (2006), Nitrogen cycling in the Middle Atlantic Bight: Results from a three-dimensional model and implications for the North Atlantic nitrogen budget, *Global Biogeochem. Cycles*, *20*, GB3007, doi:10.1029/2005GB002456.

Fennel, K., J. Wilkin, M. Previdi, and R. Najjar (2008), Denitrification effects on air-sea CO_2 flux in the coastal ocean: Simulations for the northwest North Atlantic, *Geophys. Res. Lett.*, *35*, L24608, doi:10.1029/2008GL036147.

Forster, P., et al. (2007), Changes in atmospheric constituents and in radiative forcing, in *Climate Change 2007: The Physical Science Basis. Contribution of Working Group I to the Fourth Assessment Report of the Intergovernmental Panel on Climate Change*, edited by S. Solomon et al., Cambridge Univ. Press, New York.

Frankignoulle, M., and A. V. Borges (2001), European continental shelf as a significant sink for atmospheric carbon dioxide, *Global Biogeochem. Cycles*, *15*, 569–576, doi:10.1029/2000GB001307.

Friedlingstein, P., et al. (2006), Climate-carbon cycle feedback analysis: Results from the C^4MIP model intercomparison, *J. Clim.*, *19*, 3337–3353, doi:10.1175/JCLI3800.1.

Gattuso, J.-P., M. Frankignoulle, and R. Wollast (1998), Carbon and carbonate metabolism in coastal aquatic ecosystems, *Annu. Rev. Ecol. Syst.*, *29*, 405–434, doi:10.1146/annurev.ecolsys.29.1.405.

Haidvogel, D. B., et al. (2008), Ocean forecasting in terrain-following coordinates: Formulation and skill assessment of the Regional Ocean Modeling System, *J. Comput. Phys.*, *227*, 3595–3624, doi:10.1016/j.jcp.2007.06.016.

Hurrell, J. W., Y. Kushnir, G. Ottersen, and M. Visbeck (2003), An overview of the North Atlantic Oscillation, in *The North Atlantic Oscillation: Climatic Significance and Environmental Impact*, *Geophys. Monogr. Ser.*, vol. 134, edited by J. W. Hurrell et al., pp. 1–35, AGU, Washington, D. C.

Jiang, L.-Q., W.-J. Cai, R. Wanninkhof, Y. Wang, and H. Lüger (2008), Air-sea CO_2 fluxes on the U.S. South Atlantic Bight: Spatial and seasonal variability, *J. Geophys. Res.*, *113*, C07019, doi:10.1029/2007JC004366.

Meehl, G. A., et al. (2007), Global climate projections, in *Climate Change 2007: The Physical Science Basis. Contribution of Working Group I to the Fourth Assessment Report of the Intergovernmental Panel on Climate Change*, edited by S. Solomon et al., Cambridge Univ. Press, New York.

Mellor, G. L., and T. Yamada (1982), Development of a turbulence closure model for geophysical fluid problems, *Rev. Geophys.*, *20*, 851–875, doi:10.1029/RG020i004p00851.

Millero, F. J., K. Lee, and M. Roche (1998), Distribution of alkalinity in the surface waters of the major oceans, *Mar. Chem.*, *60*, 111–130, doi:10.1016/S0304-4203(97)00084-4.

O'Reilly, J. E., and C. Zetlin (1998), Seasonal, horizontal, and vertical distribution of phytoplankton chlorophyll a in the northeast U.S. continental shelf ecosystem, U.S. Dep. of Commer., Seattle, Wash.

Salisbury, J., D. Vandemark, C. Hunt, J. Campbell, W. R. McGillis, and W. McDowell (2008), Seasonal observations of surface waters in two Gulf of Maine estuary-plume systems: Relationships between watershed attributes, optical measurements and surface pCO_2, *Estuarine Coastal Shelf Sci.*, *77*, 245–252, doi:10.1016/j.ecss.2007.09.033.

Sarmiento, J. L., and N. Gruber (2002), Sinks for anthropogenic carbon, *Phys. Today*, *55*, 30–36, doi:10.1063/1.1510279.

Sarmiento, J. L., et al. (2004), Response of ocean ecosystems to climate warming, *Global Biogeochem. Cycles*, *18*, GB3003, doi:10.1029/2003GB002134.

Takahashi, T., et al. (2002), Global sea-air CO_2 flux based on climatological surface ocean pCO_2, and seasonal biological and temperature effects, *Deep Sea Res., Part II*, *49*, 1601–1622, doi:10.1016/S0967-0645(02)00003-6.

Thomas, H., Y. Bozec, K. Elkalay, and H. J. W. de Baar (2004), Enhanced open ocean storage of CO_2 from shelf sea pumping, *Science*, *304*, 1005–1008, doi:10.1126/science.1095491.

Thomas, H., A. E. F. Prowe, I. D. Lima, S. C. Doney, R. Wanninkhof, R. J. Greatbatch, U. Schuster, and A. Corbière (2008), Changes in the North Atlantic Oscillation influence CO_2 uptake in the North Atlantic over the past 2 decades, *Global Biogeochem. Cycles*, *22*, GB4027, doi:10.1029/2007GB003167.

Trenberth, K. E., et al. (2007), Observations: surface and atmospheric climate change, in *Climate Change 2007: The Physical Science Basis. Contribution of Working Group I to the Fourth Assessment Report of the Intergovernmental Panel on Climate Change*, edited by S. Solomon et al., Cambridge Univ. Press, New York.

Tsunogai, S., S. Watanabe, and T. Sato (1999), Is there a "continental shelf pump" for the absorption of atmospheric CO_2?, *Tellus, Ser. B*, *51*, 701–712.

Uppala, S. M., et al. (2005), The ERA-40 re-analysis, *Q. J. R. Meteorol. Soc.*, *131*, 2961–3012, doi:10.1256/qj.04.176.

Verity, P. G., J. E. Bauer, C. N. Flagg, D. J. DeMaster, and D. J. Repeta (2002), The Ocean Margins Program: An interdisciplinary study of carbon sources, transformations, and sinks in a temperate continental margin system, *Deep Sea Res., Part II*, *49*, 4273–4295, doi:10.1016/S0967-0645(02)00120-0.

Walsh, J., P. Biscaye, and G. Csanady (1988), The 1983–1984 Shelf Edge Exchange Processes (SEEP)-I experiment: Hypotheses and highlights, *Cont. Shelf Res.*, *8*, 435–456, doi:10.1016/0278-4343(88)90063-5.

Wang, Z. A., W.-J. Cai, Y. Wang, and H. Ji (2005), The southeastern continental shelf of the United States as an atmospheric CO_2 source and an exporter of inorganic carbon to the ocean, *Cont. Shelf Res.*, *25*, 1917–1941, doi:10.1016/j.csr.2004.10.013.

Wanninkhof, R. (1992), Relationship between gas exchange and wind speed over the ocean, *J. Geophys. Res.*, *97*, 7373–7381, doi:10.1029/92JC00188.

Wetherald, R. T., and S. Manabe (1988), Cloud feedback processes in a general circulation model, *J. Atmos. Sci.*, *45*, 1397–1415, doi:10.1175/1520-0469(1988)045<1397:CFPIAG>2.0.CO;2.

Zeebe, R., and D. Wolf-Gladrow (2001), *CO_2 in Seawater: Equilibrium, Kinetics, Isotopes*, Elsevier, Amsterdam.

K. Fennel, Department of Oceanography, Dalhousie University, Halifax, NS B3H 4J1, Canada.

D. Haidvogel and J. Wilkin, Institute of Marine and Coastal Sciences, Rutgers University, New Brunswick, NJ 08901, USA.

M. Previdi, Lamont-Doherty Earth Observatory, Columbia University, 61 Route 9W, Palisades, NY 10964, USA. (mprevidi@ldeo.columbia.edu)